

1 Submitted to *Neural Computation*

2 Direct Learning of Sparse Changes in
3 Markov Networks by Density Ratio Estimation*

4 Song Liu

song@sg.cs.titech.ac.jp

Tokyo Institute of Technology,
2-12-1 O-okayama, Meguro, Tokyo 152-8552, Japan.
<http://sugiyama-www.cs.titech.ac.jp/~song/>

John A. Quinn

jquinn@cit.ac.ug

Makerere University, P.O. Box 7062, Kampala, Uganda.

Michael U. Gutmann

michael.gutmann@helsinki.fi

University of Helsinki, Finland, P.O. Box 68, FI-00014, Finland.

Taiji Suzuki

suzuki.t.ct@m.titech.ac.jp

Tokyo Institute of Technology,
2-12-1 O-okayama, Meguro, Tokyo 152-8552, Japan.

Masashi Sugiyama

sugi@cs.titech.ac.jp

Tokyo Institute of Technology,
2-12-1 O-okayama, Meguro, Tokyo 152-8552, Japan.
<http://sugiyama-www.cs.titech.ac.jp/>

5 **Abstract**

6 We propose a new method for detecting changes in Markov network structure be-
7 tween two sets of samples. Instead of naively fitting two Markov network models
8 separately to the two data sets and figuring out their difference, we *directly* learn the
9 network structure change by estimating the ratio of Markov network models. This
10 density-ratio formulation naturally allows us to introduce sparsity in the network
11 structure change, which highly contributes to enhancing interpretability. Further-
12 more, computation of the normalization term, which is a critical bottleneck of the
13 naive approach, can be remarkably mitigated. We also give the dual formulation
14 of the optimization problem, which further reduces the computation cost for large-
15 scale Markov networks. Through experiments, we demonstrate the usefulness of our
16 method.

*An earlier version of this work was presented at the European Conference on Machine Learning and Principles and Practice of Knowledge Discovery in Databases (ECML/PKDD2013) on Sep. 23-27, 2013.

1 Introduction

Changes in interactions between random variables are interesting in many real-world phenomena. For example, genes may interact with each other in different ways when external stimuli change, co-occurrence between words may appear/disappear when the domains of text corpora shift, and correlation among pixels may change when a surveillance camera captures anomalous activities. Discovering such changes in interactions is a task of great interest in machine learning and data mining, because it provides useful insights into underlying mechanisms in many real-world applications.

In this paper, we consider the problem of detecting changes in conditional independence among random variables between two sets of data. Such conditional independence structure can be expressed via an undirected graphical model called a *Markov network* (MN) (Bishop, 2006; Wainwright and Jordan, 2008; Koller and Friedman, 2009), where nodes and edges represent variables and their conditional dependencies, respectively. As a simple and widely applicable case, the pairwise MN model has been thoroughly studied recently (Ravikumar et al., 2010; Lee et al., 2007). Following this line, we also focus on the pairwise MN model as a representative example.

A naive approach to change detection in MNs is the two-step procedure of first estimating two MNs separately from two sets of data by *maximum likelihood estimation* (MLE), and then comparing the structure of the learned MNs. However, MLE is often computationally intractable due to the normalization factor included in the density model. Therefore, Gaussianity is often assumed in practice for computing the normalization factor analytically (Hastie et al., 2001), though this Gaussian assumption is highly restrictive in practice. We may utilize *importance sampling* (Robert and Casella, 2005) to numerically compute the normalization factor, but an inappropriate choice of the instrumental distribution may lead to an estimate with high variance (Wasserman, 2010); for more discussions on sampling techniques, see Gelman (1995) and Hinton (2002). Hyvärinen (2005) and Gutmann and Hyvärinen (2012) have explored an alternative approach to avoid computing the normalization factor which are not based on MLE.

However, the two-step procedure has the conceptual weakness that structure change is not directly learned. This indirect nature causes a crucial problem: Suppose that we want to learn a sparse structure change. For learning sparse changes, we may utilize ℓ_1 -regularized MLE (Banerjee et al., 2008; Friedman et al., 2008; Lee et al., 2007), which produces sparse MNs and thus the change between MNs also becomes sparse. However, this approach does not work if each MN is dense but only change is sparse.

To mitigate this indirect nature, the *fused-lasso* (Tibshirani et al., 2005) is useful, where two MNs are simultaneously learned with a sparsity-inducing penalty on the *difference* between two MN parameters (Zhang and Wang, 2010; Danaher et al., 2013). Although this fused-lasso approach allows us to learn sparse structure change naturally, the restrictive Gaussian assumption is still necessary to obtain the solution in a computationally tractable way.

The *nonparanormal* assumption (Liu et al., 2009, 2012) is a useful generalization of the Gaussian assumption. A nonparanormal distribution is a *semi-parametric Gaussian*

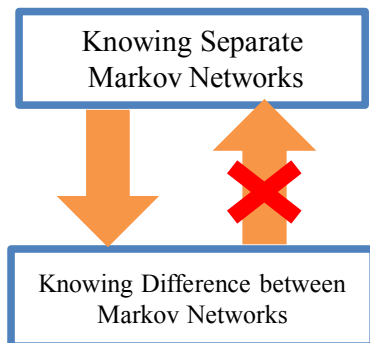


Figure 1: The rationale of direct structural change learning: finding the difference between two MNs is a more specific task than finding the entire structures of those two networks, and hence should be possible to learn with less data.

59 *copula* where each Gaussian variable is transformed by a monotone non-linear function.
 60 Nonparanormal distributions are much more flexible than Gaussian distributions thanks
 61 to the feature-wise non-linear transformation, while the normalization factors can still
 62 be computed analytically. Thus, the fused-lasso method combined with nonparanormal
 63 models would be one of the state-of-the-art approaches to change detection in MNs.
 64 However, the fused-lasso method is still based on separate modeling of two MNs, and its
 65 computation for more general non-Gaussian distributions is challenging.

66 In this paper, we propose a more direct approach to structural change learning in MNs
 67 based on *density ratio estimation* (DRE) (Sugiyama et al., 2012a). Our method does not
 68 separately model two MNs, but directly models the *change* in two MNs. This idea follows
 69 Vapnik’s principle (Vapnik, 1998):

70 If you possess a restricted amount of information for solving some problem,
 71 try to solve the problem directly and never solve a more general problem as
 72 an intermediate step. It is possible that the available information is sufficient
 73 for a direct solution but is insufficient for solving a more general intermediate
 74 problem.

75 This principle was used in the development of *support vector machines* (SVMs): rather
 76 than modeling two classes of samples, SVM directly learns a decision boundary that is
 77 sufficient for performing pattern recognition. In the current context, estimating two MNs
 78 is more general than detecting changes in MNs (Figure 1). By directly detecting changes
 79 in MNs, we can also halve the number of parameters, from two MNs to one MN-difference.

80 Another important advantage of our DRE-based method is that the normalization
 81 factor can be approximated efficiently, because the normalization term in a density ratio
 82 function takes the form of the expectation over a data distribution and thus it can be
 83 simply approximated by the sample average without additional sampling. Through ex-
 84 periments on gene expression and Twitter data analysis, we demonstrate the usefulness
 85 of our proposed approach.

86 The remainder of this paper is structured as follows. In Section 2, we formulate the
 87 problem of detecting structural changes and review currently available approaches. We
 88 then propose our DRE-based structural change detection method in Section 3. Results
 89 of illustrative and real-world experiments are reported in Section 4 and Section 5, respec-
 90 tively. Finally, we conclude our work and show the future direction in Section 6.

91 2 Problem Formulation and Related Methods

92 In this section, we formulate the problem of change detection in Markov network structure
 93 and review existing approaches.

94 2.1 Problem Formulation

Consider two sets of independent samples drawn separately from two probability distri-
 butions P and Q on \mathbb{R}^d :

$$\{\mathbf{x}_i^P\}_{i=1}^{n_P} \stackrel{\text{i.i.d.}}{\sim} P \text{ and } \{\mathbf{x}_i^Q\}_{i=1}^{n_Q} \stackrel{\text{i.i.d.}}{\sim} Q.$$

We assume that P and Q belong to the family of *Markov networks* (MNs) consisting of
 univariate and bivariate factors¹, i.e., their respective probability densities p and q are
 expressed as

$$p(\mathbf{x}; \boldsymbol{\theta}) = \frac{1}{Z(\boldsymbol{\theta})} \exp \left(\sum_{u,v=1, u \geq v}^d \boldsymbol{\theta}_{u,v}^\top \mathbf{f}(x^{(u)}, x^{(v)}) \right), \quad (1)$$

where $\mathbf{x} = (x^{(1)}, \dots, x^{(d)})^\top$ is the d -dimensional random variable, \top denotes the transpose,
 $\boldsymbol{\theta}_{u,v}$ is the parameter vector for the elements $x^{(u)}$ and $x^{(v)}$, and

$$\boldsymbol{\theta} = (\boldsymbol{\theta}_{1,1}^\top, \dots, \boldsymbol{\theta}_{d,1}^\top, \boldsymbol{\theta}_{2,2}^\top, \dots, \boldsymbol{\theta}_{d,2}^\top, \dots, \boldsymbol{\theta}_{d,d}^\top)^\top$$

is the entire parameter vector. $\mathbf{f}(x^{(u)}, x^{(v)})$ is a bivariate vector-valued basis function.
 $Z(\boldsymbol{\theta})$ is the normalization factor defined as

$$Z(\boldsymbol{\theta}) = \int \exp \left(\sum_{u,v=1, u \geq v}^d \boldsymbol{\theta}_{u,v}^\top \mathbf{f}(x^{(u)}, x^{(v)}) \right) d\mathbf{x}.$$

95 $q(\mathbf{x}; \boldsymbol{\theta})$ is defined in the same way.

96 Given two densities which can be parameterized using $p(\mathbf{x}; \boldsymbol{\theta}^P)$ and $q(\mathbf{x}; \boldsymbol{\theta}^Q)$, our goal
 97 is to discover *the changes in parameters* from P to Q , i.e., $\boldsymbol{\theta}^P - \boldsymbol{\theta}^Q$.

¹ Note that the proposed algorithm itself can be applied to *any* MNs containing more than two
 elements in each factor.

2.2 Sparse Maximum Likelihood Estimation and Graphical Lasso

Maximum likelihood estimation (MLE) with group ℓ_1 -regularization has been widely used for estimating the sparse structure of MNs (Schmidt and Murphy, 2010; Ravikumar et al., 2010; Lee et al., 2007):

$$\max_{\boldsymbol{\theta}} \left[\frac{1}{n_P} \sum_{i=1}^{n_P} \log p(\mathbf{x}_i^P; \boldsymbol{\theta}) - \lambda \sum_{u,v=1, u \geq v}^d \|\boldsymbol{\theta}_{u,v}\| \right], \quad (2)$$

where $\|\cdot\|$ denotes the ℓ_2 -norm. As λ increases, $\|\boldsymbol{\theta}_{u,v}\|$ may drop to 0. Thus, this method favors an MN that encodes more conditional independencies among variables.

Computation of the normalization term $Z(\boldsymbol{\theta})$ in Eq.(??) is often computationally intractable when the dimensionality of \mathbf{x} is high. To avoid this computational problem, the Gaussian assumption is often imposed (Friedman et al., 2008; Meinshausen and Bühlmann, 2006). More specifically, the following zero-mean Gaussian model is used:

$$p(\mathbf{x}; \boldsymbol{\Theta}) = \frac{\det(\boldsymbol{\Theta})^{1/2}}{(2\pi)^{d/2}} \exp\left(-\frac{1}{2} \mathbf{x}^\top \boldsymbol{\Theta} \mathbf{x}\right),$$

where $\boldsymbol{\Theta}$ is the inverse covariance matrix (a.k.a. the precision matrix) and $\det(\cdot)$ denotes the determinant. Then $\boldsymbol{\Theta}$ is learned as

$$\max_{\boldsymbol{\Theta}} [\log \det(\boldsymbol{\Theta}) - \text{tr}(\boldsymbol{\Theta} \mathbf{S}^P) - \lambda \|\boldsymbol{\Theta}\|_1],$$

where \mathbf{S}^P is the sample covariance matrix of $\{\mathbf{x}_i^P\}_{i=1}^n$. $\|\boldsymbol{\Theta}\|_1$ is the ℓ_1 -norm of $\boldsymbol{\Theta}$, i.e., the absolute sum of all elements. This formulation has been studied intensively in Banerjee et al. (2008), and a computationally efficient algorithm called the *graphical lasso* (Glasso) has been proposed (Friedman et al., 2008).

Sparse changes in conditional independence structure between P and Q can be detected by comparing two MNs estimated separately using sparse MLE. However, this approach implicitly assumes that two MNs are sparse, which is not necessarily true even if the change is sparse.

2.3 Fused-Lasso (Flasso) Method

To more naturally handle sparse changes in conditional independence structure between P and Q , a method based on *fused-lasso* (Tibshirani et al., 2005) has been developed (Zhang and Wang, 2010). This method directly sparsifies the *difference* between parameters.

The original method conducts *feature-wise neighborhood regression* (Meinshausen and Bühlmann, 2006) jointly for P and Q , which can be conceptually understood as maximizing the local conditional Gaussian likelihood jointly on each

feature (Ravikumar et al., 2010). A slightly more general form of the learning criterion may be summarized as

$$\max_{\boldsymbol{\theta}_s^P, \boldsymbol{\theta}_s^Q} [\ell_s^P(\boldsymbol{\theta}_s^P) + \ell_s^Q(\boldsymbol{\theta}_s^Q) - \lambda_1(\|\boldsymbol{\theta}_s^P\|_1 + \|\boldsymbol{\theta}_s^Q\|_1) - \lambda_2\|\boldsymbol{\theta}_s^P - \boldsymbol{\theta}_s^Q\|_1],$$

where $\ell_s^P(\boldsymbol{\theta})$ is the log conditional likelihood for the s -th element $x^{(s)} \in \mathbb{R}$ given the rest $\mathbf{x}^{(-s)} \in \mathbb{R}^{d-1}$:

$$\ell_s^P(\boldsymbol{\theta}) = \frac{1}{n_P} \sum_{i=1}^{n_P} \log p(x_i^{(s)P} | \mathbf{x}_i^{(-s)P}; \boldsymbol{\theta}).$$

115 $\ell_s^Q(\boldsymbol{\theta})$ is defined in the same way as $\ell_s^P(\boldsymbol{\theta})$.

116 Since the Flasso-based method directly sparsifies the change in MN structure, it can
117 work well even when each MN is not sparse. However, using other models than Gaussian
118 is difficult because of the normalization issue described in Section 2.2.

119 2.4 Nonparanormal Extensions

120 In the above methods, Gaussianity is required in practice to compute the normalization
121 factor efficiently, which is a highly restrictive assumption. To overcome this restriction,
122 it has become popular to perform structure learning under the *nonparanormal* settings
123 (Liu et al., 2009, 2012), where the Gaussian distribution is replaced by a *semi-parametric*
124 *Gaussian copula*.

125 A random vector $\mathbf{x} = (x^{(1)}, \dots, x^{(d)})^\top$ is said to follow a *nonparanormal* distribu-
126 tion, if there exists a set of monotone and differentiable functions, $\{h_i(x)\}_{i=1}^d$, such that
127 $\mathbf{h}(\mathbf{x}) = (h_1(x^{(1)}), \dots, h_d(x^{(d)}))^\top$ follows the Gaussian distribution. Nonparanormal dis-
128 tributions are much more flexible than Gaussian distributions thanks to the non-linear
129 transformation $\{h_i(x)\}_{i=1}^d$, while the normalization factors can still be computed in an
130 analytical way.

131 However, the nonparanormal transformation is restricted to be element-wise, which is
132 still restrictive to express complex distributions.

133 2.5 Maximum Likelihood Estimation for Non-Gaussian Models 134 by Importance-Sampling

135 A numerical way to obtain the MLE solution under general non-Gaussian distributions is
136 *importance sampling*.

Suppose that we try to maximize the log-likelihood²:

$$\begin{aligned} \ell_{\text{MLE}}(\boldsymbol{\theta}) &= \frac{1}{n_P} \sum_{i=1}^{n_P} \log p(\mathbf{x}_i^P; \boldsymbol{\theta}) \\ &= \frac{1}{n_P} \sum_{i=1}^{n_P} \sum_{u \geq v} \boldsymbol{\theta}_{u,v}^\top \mathbf{f}(x_i^{(u)P}, x_i^{(v)P}) - \log \int \exp \left(\sum_{u \geq v} \boldsymbol{\theta}_{u,v}^\top \mathbf{f}(x^{(u)}, x^{(v)}) \right) d\mathbf{x}. \end{aligned} \quad (3)$$

The key idea of importance sampling is to compute the integral by the expectation over an easy-to-sample *instrumental density* $p'(\mathbf{x})$ (e.g., Gaussian) weighted according to the *importance* $1/p'(\mathbf{x})$. More specifically, using i.i.d. samples $\{\mathbf{x}'_i\}_{i=1}^{n'} \stackrel{\text{i.i.d.}}{\sim} p'(\mathbf{x})$, the last term of Eq.(??) can be approximately computed as follows:

$$\begin{aligned} \log \int \exp \left(\sum_{u \geq v} \boldsymbol{\theta}_{u,v}^\top \mathbf{f}(x^{(u)}, x^{(v)}) \right) d\mathbf{x} &= \log \int p'(\mathbf{x}) \frac{\exp \left(\sum_{u \geq v} \boldsymbol{\theta}_{u,v}^\top \mathbf{f}(x^{(u)}, x^{(v)}) \right)}{p'(\mathbf{x})} d\mathbf{x} \\ &\approx \log \frac{1}{n'} \sum_{i=1}^{n'} \frac{\exp \left(\sum_{u \geq v} \boldsymbol{\theta}_{u,v}^\top \mathbf{f}(x_i'^{(u)}, x_i'^{(v)}) \right)}{p'(\mathbf{x}'_i)}. \end{aligned}$$

137 We refer to this implementation of Glasso as IS-Glasso below.

138 However, importance sampling tends to produce an estimate with large variance if the
139 instrumental distribution is not carefully chosen. Although it is often suggested to use a
140 density whose shape is similar to the function to be integrated but with thicker tails as
141 p' , it is not straightforward in practice to decide which p' to choose, especially when the
142 dimensionality of \mathbf{x} is high (Wasserman, 2010).

We can also consider an importance-sampling version of the Flasso method (which we refer to as IS-Flasso)³

$$\max_{\boldsymbol{\theta}^P, \boldsymbol{\theta}^Q} \left[\ell_{\text{MLE}}^P(\boldsymbol{\theta}^P) + \ell_{\text{MLE}}^Q(\boldsymbol{\theta}^Q) - \lambda_1 (\|\boldsymbol{\theta}^P\|^2 + \|\boldsymbol{\theta}^Q\|^2) - \lambda_2 \sum_{u \geq v} \|\boldsymbol{\theta}_{u,v}^P - \boldsymbol{\theta}_{u,v}^Q\| \right],$$

143 where both $\ell_{\text{MLE}}^P(\boldsymbol{\theta}^P)$ and $\ell_{\text{MLE}}^Q(\boldsymbol{\theta}^Q)$ are approximated by importance sampling for non-
144 Gaussian distributions. However, in the same way as IS-Glasso, the choice of instrumental
145 distributions is not straightforward.

146 3 Direct Learning of Structural Changes via Density 147 Ratio Estimation

148 The Flasso method can more naturally handle sparse changes in MNs than separate sparse
149 MLE. However, the Flasso method is still based on separate modeling of two MNs, and

²From here on, we simplify $\sum_{u,v=1, u \geq v}^d$ as $\sum_{u \geq v}$.

³For implementation simplicity, we maximize the joint likelihood of p and q , instead of its feature-wise conditional likelihood. We also switch the first penalty term from ℓ_1 to ℓ_2 .

150 its computation for general high-dimensional non-Gaussian distributions is challenging.
 151 In this section, we propose to directly learn structural changes based on *density ratio*
 152 *estimation* (Sugiyama et al., 2012a). Our approach does not involve separate modeling
 153 of each MN and allows us to approximate the normalization term efficiently for *any*
 154 distributions.

155 3.1 Density Ratio Formulation for Structural Change Detection

156 Our key idea is to consider the ratio of p and q :

$$\frac{p(\mathbf{x}; \boldsymbol{\theta}^P)}{q(\mathbf{x}; \boldsymbol{\theta}^Q)} \propto \exp \left(\sum_{u \geq v} (\boldsymbol{\theta}_{u,v}^P - \boldsymbol{\theta}_{u,v}^Q)^\top \mathbf{f}(x^{(u)}, x^{(v)}) \right).$$

157 Here $\boldsymbol{\theta}_{u,v}^P - \boldsymbol{\theta}_{u,v}^Q$ encodes the difference between P and Q for factor $\mathbf{f}(x^{(u)}, x^{(v)})$, i.e.,
 158 $\boldsymbol{\theta}_{u,v}^P - \boldsymbol{\theta}_{u,v}^Q$ is zero if there is no change in the factor $\mathbf{f}(x^{(u)}, x^{(v)})$.

Once we consider the ratio of p and q , we actually do not have to estimate $\boldsymbol{\theta}_{u,v}^P$ and
 $\boldsymbol{\theta}_{u,v}^Q$; instead estimating their difference $\boldsymbol{\theta}_{u,v} = \boldsymbol{\theta}_{u,v}^P - \boldsymbol{\theta}_{u,v}^Q$ is sufficient for change detection:

$$r(\mathbf{x}; \boldsymbol{\theta}) = \frac{1}{N(\boldsymbol{\theta})} \exp \left(\sum_{u \geq v} \boldsymbol{\theta}_{u,v}^\top \mathbf{f}(x^{(u)}, x^{(v)}) \right), \quad (4)$$

where

$$N(\boldsymbol{\theta}) = \int q(\mathbf{x}) \exp \left(\sum_{u \geq v} \boldsymbol{\theta}_{u,v}^\top \mathbf{f}(x^{(u)}, x^{(v)}) \right) d\mathbf{x}.$$

The normalization term $N(\boldsymbol{\theta})$ guarantees⁴

$$\int q(\mathbf{x}) r(\mathbf{x}; \boldsymbol{\theta}) d\mathbf{x} = 1.$$

⁴ If the model $q(\mathbf{x}; \boldsymbol{\theta}^Q)$ is correctly specified, i.e., there exists $\boldsymbol{\theta}^{Q^*}$ such that $q(\mathbf{x}; \boldsymbol{\theta}^{Q^*}) = q(\mathbf{x})$, then $N(\boldsymbol{\theta})$ can be interpreted as importance sampling of $Z(\boldsymbol{\theta}^P)$ via instrumental distribution $q(\mathbf{x})$. Indeed, since

$$Z(\boldsymbol{\theta}^P) = \int q(\mathbf{x}) \frac{\exp \left(\sum_{u \geq v} \boldsymbol{\theta}_{u,v}^P \cdot \mathbf{f}(x^{(u)}, x^{(v)}) \right)}{q(\mathbf{x}; \boldsymbol{\theta}^{Q^*})} d\mathbf{x},$$

where $q(\mathbf{x}; \boldsymbol{\theta}^{Q^*}) = q(\mathbf{x})$, we have

$$N(\boldsymbol{\theta}^P - \boldsymbol{\theta}^{Q^*}) = \frac{Z(\boldsymbol{\theta}^P)}{Z(\boldsymbol{\theta}^{Q^*})} = \int q(\mathbf{x}) \exp \left(\sum_{u \geq v} (\boldsymbol{\theta}_{u,v}^P - \boldsymbol{\theta}_{u,v}^{Q^*})^\top \mathbf{f}(x^{(u)}, x^{(v)}) \right) d\mathbf{x}.$$

This is exactly the normalization term $N(\boldsymbol{\theta})$ of the ratio $p(\mathbf{x}; \boldsymbol{\theta}^P)/q(\mathbf{x}; \boldsymbol{\theta}^{Q^*})$. However, we note that the density ratio estimation method we use in this paper is consistent to the optimal solution in the model

159 Thus, in this density ratio formulation, we are no longer modeling p and q separately,
 160 but we model the change from p to q *directly*. This direct nature would be more suitable
 161 for change detection purposes according to Vapnik’s principle that encourages avoidance
 162 of solving more general problems as an intermediate step (Vapnik, 1998). This direct
 163 formulation also allows us to halve the number of parameters from both $\boldsymbol{\theta}^P$ and $\boldsymbol{\theta}^Q$ to
 164 only $\boldsymbol{\theta}$.

Furthermore, the normalization factor $N(\boldsymbol{\theta})$ in the density ratio formulation can be easily approximated by the sample average over $\{\mathbf{x}_i^Q\}_{i=1}^{n_Q} \stackrel{\text{i.i.d.}}{\sim} q(\mathbf{x})$, because $N(\boldsymbol{\theta})$ is the expectation over $q(\mathbf{x})$:

$$N(\boldsymbol{\theta}) \approx \frac{1}{n_Q} \sum_{i=1}^{n_Q} \exp \left(\sum_{u \geq v} \boldsymbol{\theta}_{u,v}^\top \mathbf{f}(x_i^{(u)Q}, x_i^{(v)Q}) \right).$$

165 3.2 Direct Density-Ratio Estimation

166 Density ratio estimation has been recently introduced to the machine learning community
 167 and is proven to be useful in a wide range of applications (Sugiyama et al., 2012a). Here,
 168 we concentrate on the density ratio estimator called the *Kullback-Leibler importance es-*
 169 *timation procedure* (KLIEP) for log-linear models (Sugiyama et al., 2008; Tsuboi et al.,
 170 2009).

For a density ratio model $r(\mathbf{x}; \boldsymbol{\theta})$, the KLIEP method minimizes the Kullback-Leibler divergence from $p(\mathbf{x})$ to $\hat{p}(\mathbf{x}) = q(\mathbf{x})r(\mathbf{x}; \boldsymbol{\theta})$:

$$\begin{aligned} \text{KL}[p \parallel \hat{p}] &= \int p(\mathbf{x}) \log \frac{p(\mathbf{x})}{q(\mathbf{x})r(\mathbf{x}; \boldsymbol{\theta})} d\mathbf{x} \\ &= \text{Const.} - \int p(\mathbf{x}) \log r(\mathbf{x}; \boldsymbol{\theta}) d\mathbf{x}. \end{aligned} \quad (5)$$

Note that our density-ratio model (??) automatically satisfies the non-negativity and normalization constraints:

$$r(\mathbf{x}; \boldsymbol{\theta}) \geq 0 \quad \text{and} \quad \int q(\mathbf{x})r(\mathbf{x}; \boldsymbol{\theta}) d\mathbf{x} = 1.$$

even without the correct model assumption (Kanamori et al., 2010). An alternative normalization term,

$$N'(\boldsymbol{\theta}, \boldsymbol{\theta}^Q) = \int q(\mathbf{x}; \boldsymbol{\theta}^Q)r(\mathbf{x}; \boldsymbol{\theta}) d\mathbf{x},$$

may also be considered, as in the case of MLE. However, this alternative form requires an extra parameter $\boldsymbol{\theta}^Q$ which is not our main interest.

In practice, we maximize the empirical approximation of the second term in Eq.(??):

$$\begin{aligned} \ell_{\text{KLIEP}}(\boldsymbol{\theta}) &= \frac{1}{n_P} \sum_{i=1}^{n_P} \log r(\mathbf{x}_i^P; \boldsymbol{\theta}) \\ &= \frac{1}{n_P} \sum_{i=1}^{n_P} \sum_{u \geq v} \boldsymbol{\theta}_{u,v}^\top \mathbf{f}(x_i^{(u)P}, x_i^{(v)P}) \\ &\quad - \log \left(\frac{1}{n_Q} \sum_{i=1}^{n_Q} \exp \left(\sum_{u \geq v} \boldsymbol{\theta}_{u,v}^\top \mathbf{f}(x_i^{(u)Q}, x_i^{(v)Q}) \right) \right). \end{aligned}$$

Because $\ell_{\text{KLIEP}}(\boldsymbol{\theta})$ is concave with respect to $\boldsymbol{\theta}$, its global maximizer can be numerically found by standard optimization techniques such as gradient ascent or quasi-Newton methods. The gradient of ℓ_{KLIEP} with respect to $\boldsymbol{\theta}_{u,v}$ is given by

$$\begin{aligned} \nabla_{\boldsymbol{\theta}_{u,v}} \ell_{\text{KLIEP}}(\boldsymbol{\theta}) &= \frac{1}{n_P} \sum_{i=1}^{n_P} \mathbf{f}(x_i^{(u)P}, x_i^{(v)P}) \\ &\quad - \frac{\frac{1}{n_Q} \sum_{i=1}^{n_Q} \exp \left(\sum_{u' \geq v'} \boldsymbol{\theta}_{u',v'}^\top \mathbf{f}(x_i^{(u')Q}, x_i^{(v')Q}) \right) \mathbf{f}(x_i^{(u)Q}, x_i^{(v)Q})}{\frac{1}{n_Q} \sum_{j=1}^{n_Q} \exp \left(\sum_{u'' \geq v''} \boldsymbol{\theta}_{u'',v''}^\top \mathbf{f}(x_j^{(u'')Q}, x_j^{(v'')Q}) \right)}, \end{aligned}$$

171 which can be computed in a straightforward manner for *any* feature vector $\mathbf{f}(x^{(u)}, x^{(v)})$.

172 3.3 Sparsity-Inducing Norm

173 To find a sparse change between P and Q , we propose to regularize the KLIEP solution
 174 with a sparsity-inducing norm $\sum_{u \geq v} \|\boldsymbol{\theta}_{u,v}\|$. Note that the MLE approach sparsifies both
 175 $\boldsymbol{\theta}^P$ and $\boldsymbol{\theta}^Q$ so that the difference $\boldsymbol{\theta}^P - \boldsymbol{\theta}^Q$ is also sparsified, while we directly sparsify the
 176 difference $\boldsymbol{\theta}^P - \boldsymbol{\theta}^Q$; thus our method can still work well even if $\boldsymbol{\theta}^P$ and $\boldsymbol{\theta}^Q$ are dense.

In practice, we may use the following *elastic-net* penalty (Zou and Hastie, 2005) to better control overfitting to noisy data:

$$\max_{\boldsymbol{\theta}} \left[\ell_{\text{KLIEP}}(\boldsymbol{\theta}) - \lambda_1 \|\boldsymbol{\theta}\|^2 - \lambda_2 \sum_{u \geq v} \|\boldsymbol{\theta}_{u,v}\| \right], \quad (6)$$

177 where $\|\boldsymbol{\theta}\|^2$ penalizes the magnitude of the entire parameter vector.

178 3.4 Dual Formulation for High-Dimensional Data

179 The solution of the optimization problem (??) can be easily obtained by standard sparse
 180 optimization methods. However, in the case where the input dimensionality d is high
 181 (which is often the case in our setup), the dimensionality of parameter vector $\boldsymbol{\theta}$ is large,
 182 and thus obtaining the solution can be computationally expensive. Here, we derive a

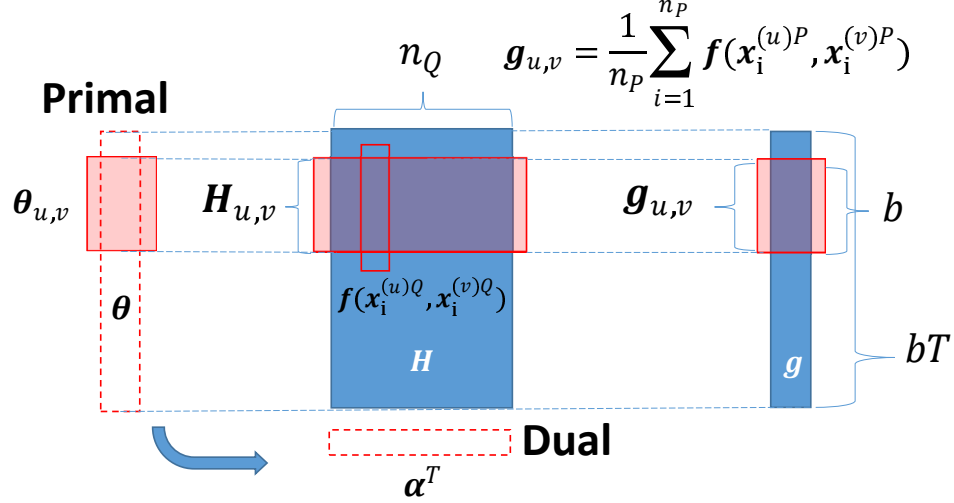


Figure 2: Schematics of primal and dual optimization. b denotes the number of basis functions and T denotes the number of factors. Because we are considering pairwise factors, $T = \mathcal{O}(d^2)$ for input dimensionality d .

183 dual optimization problem (Boyd and Vandenberghe, 2004), which can be solved more
 184 efficiently for high-dimensional θ (Figure 2).

As detailed in Appendix, the dual optimization problem is given as

$$\begin{aligned}
 \min_{\alpha=(\alpha_1, \dots, \alpha_{n_Q})^\top} & \sum_{i=1}^{n_Q} \alpha_i \log \alpha_i + \frac{1}{\lambda_1} \sum_{u \geq v} \max(0, \|\xi_{u,v}\| - \lambda_2)^2 \\
 \text{subject to } & \alpha_1, \dots, \alpha_{n_Q} \geq 0 \text{ and } \sum_{i=1}^{n_Q} \alpha_i = 1,
 \end{aligned} \tag{7}$$

where

$$\begin{aligned}
 \xi_{u,v} &= \mathbf{g}_{u,v} - \mathbf{H}_{u,v} \alpha, \\
 \mathbf{H}_{u,v} &= [\mathbf{f}(x_1^{(u)Q}, x_1^{(v)Q}), \dots, \mathbf{f}(x_{n_Q}^{(u)Q}, x_{n_Q}^{(v)Q})], \\
 \mathbf{g}_{u,v} &= \frac{1}{n_P} \sum_{i=1}^{n_P} \mathbf{f}(x_i^{(u)P}, x_i^{(v)P}).
 \end{aligned}$$

The primal solution can be obtained from the dual solution as

$$\theta_{u,v} = \begin{cases} \frac{1}{\lambda_1} \left(1 - \frac{\lambda_2}{\|\xi_{u,v}\|}\right) \xi_{u,v} & \text{if } \|\xi_{u,v}\| > \lambda_2, \\ \mathbf{0} & \text{if } \|\xi_{u,v}\| \leq \lambda_2. \end{cases} \tag{8}$$

185 Note that the dimensionality of the dual variable α is equal to n_Q , while that of
 186 θ is quadratic with respect to the input dimensionality d , because we are considering

187 pairwise factors. Thus, if d is not small and n_Q is not very large (which is often the
 188 case in our experiments shown later), solving the dual optimization problem would be
 189 computationally more efficient. Furthermore, the dual objective (and its gradient) can be
 190 computed efficiently in parallel for each (u, v) , which is a useful property when handling
 191 large-scale MNs. Note that the dual objective is differentiable everywhere, while the
 192 primal objective is not.

193 4 Numerical Experiments

194 In this section, we compare the performance of the proposed KLIEP-based method, the
 195 Flasso method, and the Glasso method for Gaussian models, nonparanormal models, and
 196 non-Gaussian models. Results are reported on datasets with three different underlying
 197 distributions: multivariate Gaussian, nonparanormal, and non-Gaussian “diamond” dis-
 198 tributions. We also investigate the computation time of the primal and dual formulations
 199 as a function of the input dimensionality. The MATLAB implementation of the primal
 200 and dual methods are available at

201 <http://sugiyama-www.cs.titech.ac.jp/~song/SCD.html>.

202 4.1 Gaussian Distribution

203 First, we investigate the performance of each method under Gaussianity.

Consider a 40-node sparse Gaussian MN, where its graphical structure is characterized
 by precision matrix Θ^P with diagonal elements equal to 2. The off-diagonal elements are
 randomly chosen⁵ and set to 0.2, so that the overall sparsity of Θ^P is 25%. We then
 introduce changes by randomly picking 15 edges and reducing the corresponding elements
 in the precision matrix by 0.1. The resulting precision matrices Θ^P and Θ^Q are used for
 drawing samples as

$$\{\mathbf{x}_i^P\}_{i=1}^{n_P} \stackrel{\text{i.i.d.}}{\sim} \mathcal{N}(\mathbf{0}, (\Theta^P)^{-1}) \quad \text{and} \quad \{\mathbf{x}_i^Q\}_{i=1}^{n_Q} \stackrel{\text{i.i.d.}}{\sim} \mathcal{N}(\mathbf{0}, (\Theta^Q)^{-1}),$$

204 where $\mathcal{N}(\boldsymbol{\mu}, \boldsymbol{\Sigma})$ denotes the multivariate normal distribution with mean $\boldsymbol{\mu}$ and covariance
 205 matrix $\boldsymbol{\Sigma}$. Datasets of size $n = n_P = n_Q = 50, 100$ are tested.

206 We compare the performance of the KLIEP, Flasso, and Glasso methods. Because all
 207 methods use the same Gaussian model, the difference in performance is caused only by
 208 the difference in estimation methods. We repeat the experiments 20 times with randomly
 209 generated datasets and report the results in Figure 3.

210 The top 6 graphs are examples of regularization paths⁶. The dashed lines represent
 211 changed edges in the ground truth, while the solid lines represent unchanged edges. The
 212 top row is for $n = 100$ while the middle row is for $n = 50$. The bottom 3 graphs are
 213 the data generating distribution and averaged precision-recall (P-R) curves with standard

⁵We set $\Theta_{u,v} = \Theta_{v,u}$ for not breaking the symmetry of the precision matrix.

⁶Paths of univariate factors are omitted for clear visibility.

214 error over 20 runs. The P-R curves are plotted by varying the group-sparsity control
 215 parameter λ_2 with $\lambda_1 = 0$ in KLIEP and Flasso, and by varying the sparsity control
 216 parameters as $\lambda = \lambda^P = \lambda^Q$ in Glasso.

217 In the regularization path plots, solid vertical lines show the regularization parameter
 218 values picked based on hold-out data $\{\tilde{\mathbf{x}}_i^P\}_{i=1}^{3000} \stackrel{\text{i.i.d.}}{\sim} P$ and $\{\tilde{\mathbf{x}}_i^Q\}_{i=1}^{3000} \stackrel{\text{i.i.d.}}{\sim} Q$ as follows:

- **KLIEP:** The *hold-out log-likelihood* (HOLL) is maximized:

$$\frac{1}{\tilde{n}_P} \sum_{i=1}^{\tilde{n}_P} \log \frac{\exp\left(\sum_{u \geq v} \hat{\boldsymbol{\theta}}_{u,v}^\top \mathbf{f}(\tilde{\mathbf{x}}_i^{(u)P}, \tilde{\mathbf{x}}_i^{(v)P})\right)}{\frac{1}{\tilde{n}_Q} \sum_{j=1}^{\tilde{n}_Q} \exp\left(\sum_{u' \geq v'} \hat{\boldsymbol{\theta}}_{u',v'}^\top \mathbf{f}(\tilde{\mathbf{x}}_j^{(u')Q}, \tilde{\mathbf{x}}_j^{(v')Q})\right)}.$$

- **Flasso:** The sum of feature-wise conditional HOLLs for $p(\mathbf{x}^{(s)} | \mathbf{x}^{(-s)}; \boldsymbol{\theta}_s)$ and $q(\mathbf{x}^{(s)} | \mathbf{x}^{(-s)}; \boldsymbol{\theta}_s)$ over all nodes is maximized:

$$\frac{1}{\tilde{n}_P} \sum_{i=1}^{\tilde{n}_P} \sum_{s=1}^d \log p(\tilde{\mathbf{x}}_i^{(s)P} | \tilde{\mathbf{x}}_i^{(-s)P}; \hat{\boldsymbol{\theta}}_s^P) + \frac{1}{\tilde{n}_Q} \sum_{i=1}^{\tilde{n}_Q} \sum_{s=1}^d \log q(\tilde{\mathbf{x}}_i^{(s)Q} | \tilde{\mathbf{x}}_i^{(-s)Q}; \hat{\boldsymbol{\theta}}_s^Q).$$

- **Glasso:** The sum of HOLLs for $p(\mathbf{x}; \boldsymbol{\theta})$ and $q(\mathbf{x}; \boldsymbol{\theta})$ is maximized:

$$\frac{1}{\tilde{n}_P} \sum_{i=1}^{\tilde{n}_P} \log p(\tilde{\mathbf{x}}_i^P; \hat{\boldsymbol{\theta}}^P) + \frac{1}{\tilde{n}_Q} \sum_{i=1}^{\tilde{n}_Q} \log q(\tilde{\mathbf{x}}_i^Q; \hat{\boldsymbol{\theta}}^Q).$$

219 When $n = 100$, KLIEP and Flasso clearly distinguish changed (dashed lines) and
 220 unchanged (solid lines) edges in terms of parameter magnitude. However, when the
 221 sample size is halved to $n = 50$, the separation is visually rather unclear in the case of
 222 Flasso. In contrast, the paths of changed and unchanged edges are still almost disjoint in
 223 the case of KLIEP. The Glasso method performs rather poorly in both cases. A similar
 224 tendency can be observed also in the P-R curve plot: When the sample size is $n = 100$,
 225 KLIEP and Flasso work equally well, but KLIEP gains its lead when the sample size is
 226 reduced to $n = 50$. Glasso does not perform well in both cases.

227 4.2 Nonparanormal Distribution

We post-process the Gaussian dataset used in Section 4.1 to construct nonparanormal samples. More specifically, we apply the power function,

$$h_i^{-1}(x) = \text{sign}(x)|x|^{\frac{1}{2}},$$

228 to each dimension of \mathbf{x}^P and \mathbf{x}^Q , so that $\mathbf{h}(\mathbf{x}^P) \sim \mathcal{N}(\mathbf{0}, (\boldsymbol{\Theta}^P)^{-1})$ and $\mathbf{h}(\mathbf{x}^Q) \sim$
 229 $\mathcal{N}(\mathbf{0}, (\boldsymbol{\Theta}^Q)^{-1})$.

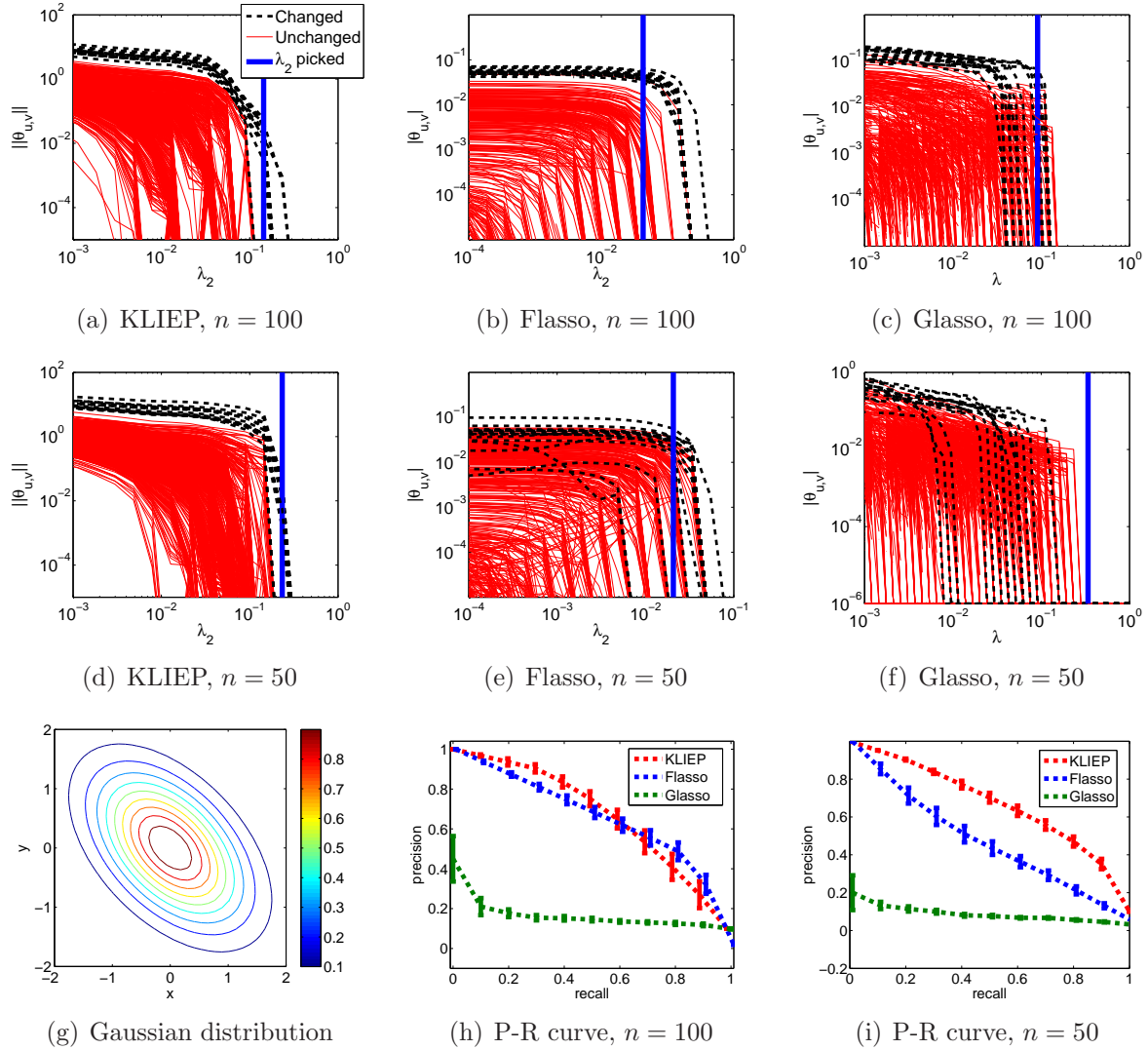


Figure 3: Experimental results on the Gaussian dataset.

To cope with the non-linearity in the KLIEP method, we use the power nonparanormal basis functions with power $k = 2, 3$, and 4:

$$\mathbf{f}(x_i, x_j) = (\text{sign}(x_i)|x_i|^k, \text{sign}(x_j)|x_j|^k, 1)^\top.$$

230 Model selection of k is performed together with the regularization parameter by HOLL
 231 maximization. For Flasso and Glasso, we apply the nonparanormal transform as described
 232 in Liu et al. (2009) before the structural change is learned.

233 The experiments are conducted on 20 randomly generated datasets with $n = 50$ and
 234 100, respectively. The regularization paths, data generating distribution, and averaged
 235 P-R curves are plotted in Figure 4. The results show that Flasso clearly suffers from the
 236 performance degradation compared with the Gaussian case, perhaps because the number

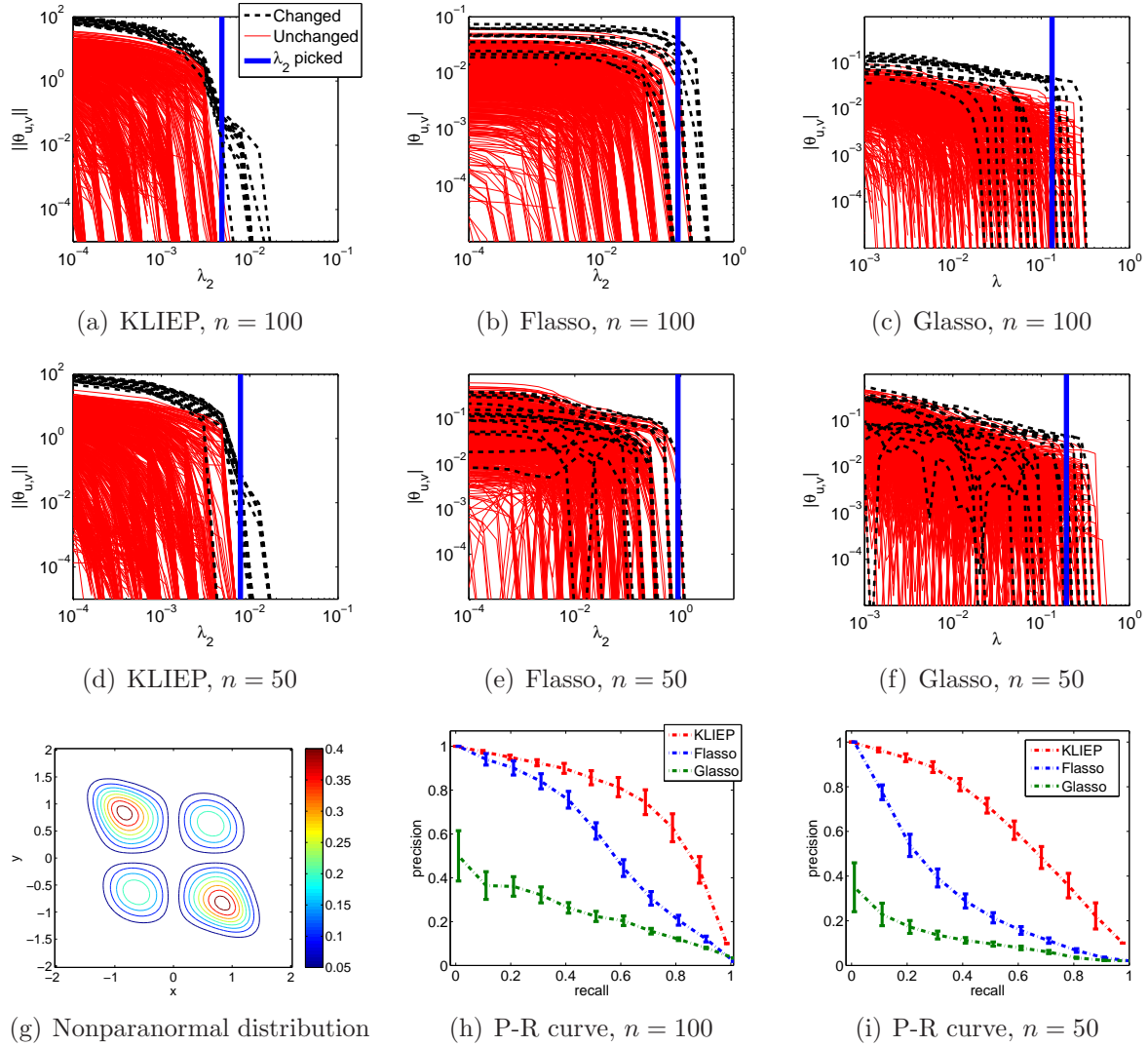


Figure 4: Experimental results on the nonparanormal dataset.

237 of samples is too small for the complicated nonparanormal distribution. Due to the two-
 238 step estimation scheme, the performance of Glasso is poor. In contrast, KLIEP separates
 239 changed and unchanged edges still clearly for both $n = 50$ and $n = 100$. The P-R curves
 240 also show the same tendency.

241 4.3 “Diamond” Distribution with No Pearson Correlation

242 In the experiments in Section 4.2, though samples are non-Gaussian, the *Pearson cor-*
 243 *relation* is not zero. Therefore, methods assuming Gaussianity can still capture some
 244 linear correlation between random variables. Here, we consider a more challenging case
 245 with a diamond-shaped distribution within the exponential family that has zero Pearson
 246 correlation between variables. Thus, the methods assuming Gaussianity cannot extract

247 any information in principle from this dataset.

The probability density function of the diamond distribution is defined as follows (Figure 5(a)):

$$p(\mathbf{x}) \propto \exp \left(- \sum_{i=1}^d 2x_i^2 - \sum_{(i,j):A_{i,j} \neq 0} 20x_i^2 x_j^2 \right), \quad (9)$$

248 where the adjacency matrix \mathbf{A} describes the MN structure. Note that this distribution
249 cannot be transformed into a Gaussian distribution by any nonparanormal transforma-
250 tions.

251 We set $d = 9$ and $n_P = n_Q = 5000$. \mathbf{A}^P is randomly generated with 35% sparsity, while
252 \mathbf{A}^Q is created by randomly removing edges in \mathbf{A}^P so that the sparsity level is dropped to
253 15%. Samples from the above distribution are drawn by using a *slice sampling* method
254 (Neal, 2003). Since generating samples from high-dimensional distributions is non-trivial
255 and time-consuming, we focus on a relatively low-dimensional case. To avoid sampling
256 error which may mislead the experimental evaluation, we also increase the sample size,
257 so that the erratic points generated by accident will not affect the overall population.

In this experiment, we compare the performance of KLIEP, Flasso, and Glasso with the Gaussian model, the power nonparanormal model, and the polynomial model:

$$\mathbf{f}(x_i, x_j) = (x_i^k, x_j^k, x_i x_j^{k-1}, \dots, x_i^{k-1} x_j, x_i^{k-1}, x_j^{k-1}, \dots, x_i, x_j, 1)^\top \text{ for } i \neq j.$$

258 The univariate polynomial transform is defined as $\mathbf{f}(x_i, x_i) = \mathbf{f}(x_i, 0)$. We test $k =$
259 $2, 3, 4$ and choose the best one in terms of HOLL. The Flasso and Glasso methods for
260 the polynomial model are computed by importance sampling, i.e., we use the IS-Flasso
261 and IS-Glasso methods (see Section 2.5). Since these methods are computationally very
262 expensive, we only test $k = 4$ which we found to be a reasonable choice. We set the
263 instrumental distribution p' as the standard normal $\mathcal{N}(\mathbf{0}, \mathbf{I})$, and use sample $\{\mathbf{x}'_i\}_{i=1}^{70000} \sim p'$
264 for approximating integrals. p' is purposely chosen so that it has a similar “bell” shape
265 to the target densities but with larger variance on each dimension.

266 The averaged P-R curves over 20 datasets are shown in Figure 5(e). KLIEP with the
267 polynomial model significantly outperforms all the other methods, while the IS-Glasso and
268 especially IS-Flasso give better result than the KLIEP, Flasso, and Glasso methods with
269 the Gaussian and nonparanormal models. This means that the polynomial basis function
270 is indeed helpful in handling completely non-Gaussian data. However, as discussed in
271 Section 2.2, it is difficult to use such a basis function in Glasso and Flasso because of
272 the computational intractability of the normalization term. Although IS-Glasso can ap-
273 proximate integrals, the result shows that such approximation of integrals does not lead
274 to a very good performance. In comparison, the result of the IS-Flasso method is much
275 improved thanks to the coupled sparsity regularization, but it is still not comparable to
276 KLIEP.

277 The regularization paths of KLIEP with the polynomial model illustrated in Fig-
278 ure 5(b) show the usefulness of the proposed method in change detection under non-
279 Gaussianity. We also give regularization paths obtained by the IS-Flasso and IS-Glasso

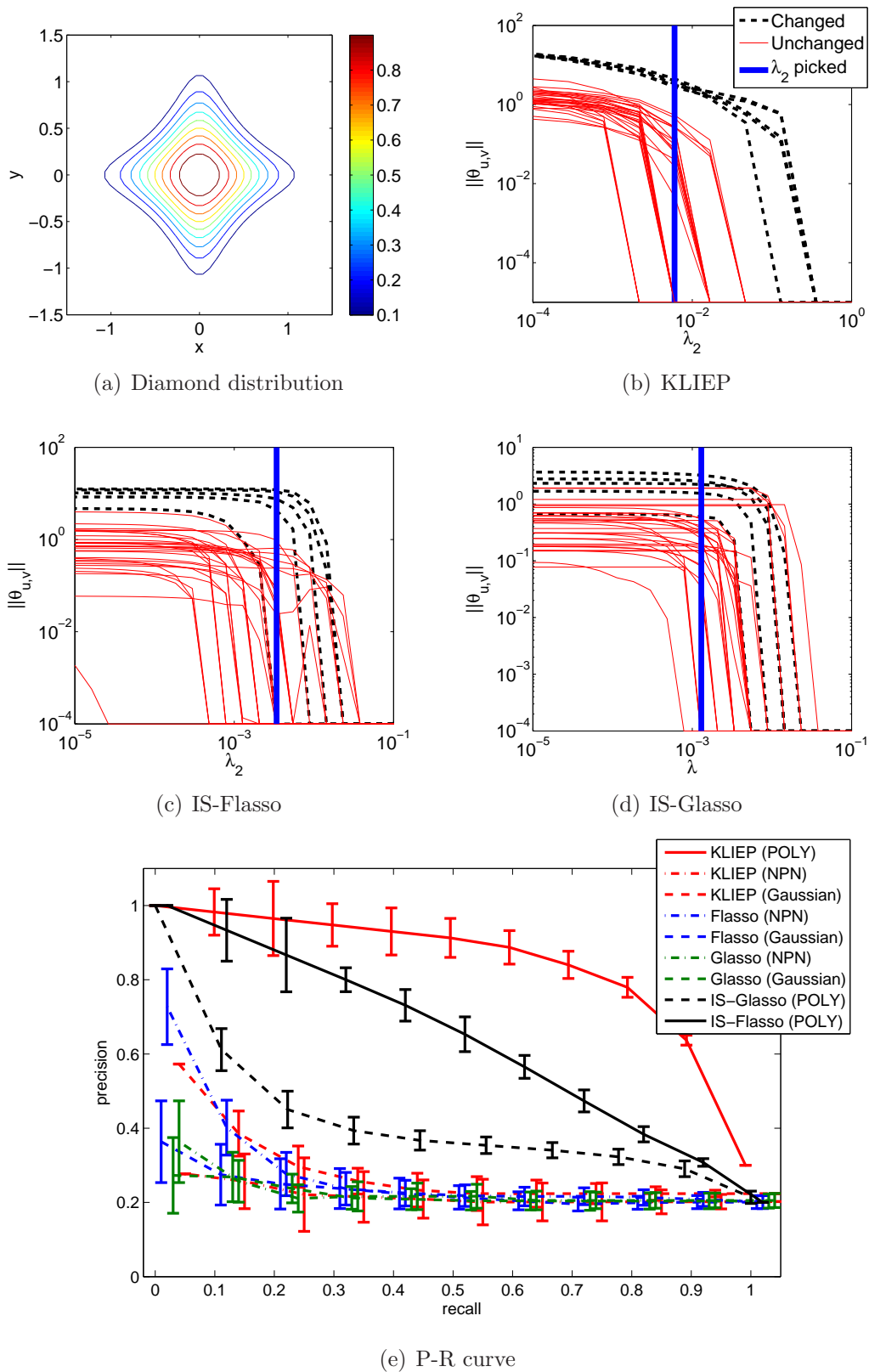


Figure 5: Experimental results on the diamond dataset. “NPN” and “POLY” denote the nonparanormal and polynomial models, respectively. Note that the precision rate of 100% recall for a random guess is approximately 20%.

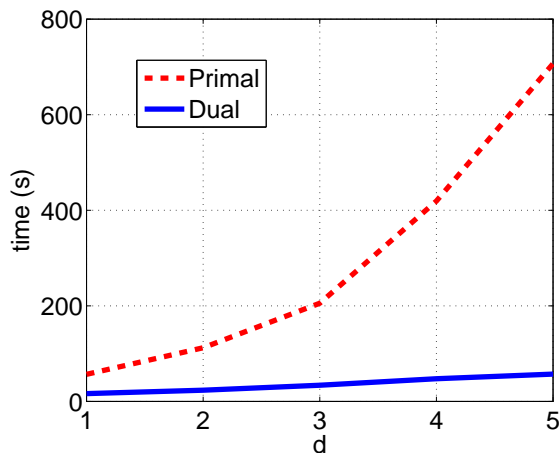


Figure 6: Comparison of computation time for solving primal and dual optimization problems.

280 methods on the same dataset in Figures 5(c) and 5(d), respectively. The graphs show that
 281 both methods do not separate changed and unchanged edges well, though the IS-Flasso
 282 method works slightly better.

283 4.4 Computation Time: Dual versus Primal Optimization Prob- 284 lems

285 Finally, we compare the computation time of the proposed KLIEP method when solving
 286 the dual optimization problem (??) and the primal optimization problem (??). Both the
 287 optimization problems are solved by using the same convex optimizer *minFunc*⁷. The
 288 datasets are generated from two Gaussian distributions constructed in the same way as
 289 Section 4.1. 150 samples are separately drawn from two distributions with dimension
 290 $d = 40, 50, 60, 70, 80$. We then perform change detection by computing the regularization
 291 paths using 20 choices of λ_2 ranging from 10^{-4} to 10^0 and fix $\lambda_1 = 0.1$. The results are
 292 plotted in Figure 6.

293 It can be seen from the graph that as the dimensionality increases, the computation
 294 time for solving the primal optimization problem is sharply increased, while that for solv-
 295 ing the dual optimization problem grows only moderately: when $d = 80$, the computation
 296 time for obtaining the primal solution is almost 10 times more than that required for
 297 obtaining the dual solution. Thus, the dual formulation is computationally much more
 298 efficient than the primal formulation.

⁷<http://www.di.ens.fr/~mschmidt/Software/minFunc.html>

5 Applications

In this section, we report the experimental results on a synthetic gene expression dataset and a Twitter dataset.

5.1 Synthetic Gene Expression Dataset

A gene regulatory network encodes interactions between DNA segments. However, the way genes interact may change due to environmental or biological stimuli. In this experiment, we focus on detecting such changes. We use *SynTReN*, which is a generator of gene regulatory networks used for benchmark validation of bioinformatics algorithms (Van den Bulcke et al., 2006).

We first choose a sub-network containing 13 nodes from an existing signaling network in *Saccharomyces cerevisiae* (shown in Figure 7(a)). Three types of interactions are modeled: activation (ac), deactivation (re), and dual (du). 50 samples are generated in the first stage, after which we change the types of interactions in 6 edges, and generate 50 samples again. Four types of changes are considered: $ac \rightarrow re$, $re \rightarrow ac$, $du \rightarrow ac$, and $du \rightarrow re$.

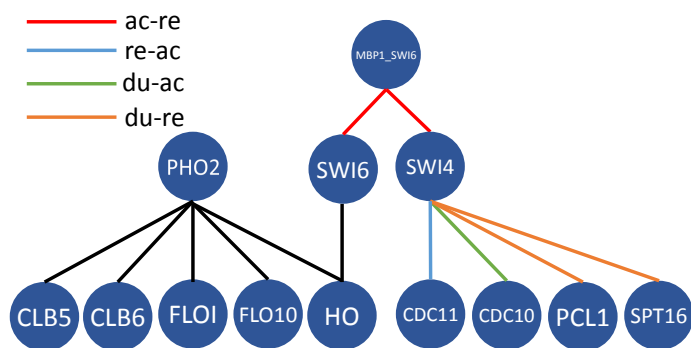
We use KLIEP and IS-Flasso with the polynomial transform function for $k \in \{2, 3, 4\}$. The regularization parameter λ_1 in KLIEP and Flasso is tested with choices $\lambda_1 \in \{0.1, 1, 10\}$. We set the instrumental distribution p' as the standard normal $\mathcal{N}(\mathbf{0}, \mathbf{I})$, and use sample $\{\mathbf{x}'_i\}_{i=1}^{70000} \sim p'$ for approximating integrals in IS-Flasso.

The regularization paths on one example dataset for KLIEP, IS-Flasso, and the plain Flasso with the Gaussian model are plotted in Figures 7(b), 7(c), and 7(d), respectively. Averaged P-R curves over 20 simulation runs are shown in Figure 7(e). We can see clearly from the KLIEP regularization paths shown in Figure 7(b) that the magnitude of estimated parameters on the changed pairwise interactions is much higher than that of the unchanged edges. IS-Flasso also achieves rather clear separation between changed and unchanged interactions, though there are a few unchanged interactions drop to zero at the final stage. Flasso gives many false alarms by assigning non-zero values to the unchanged edges, even after some changed edges hit zeros.

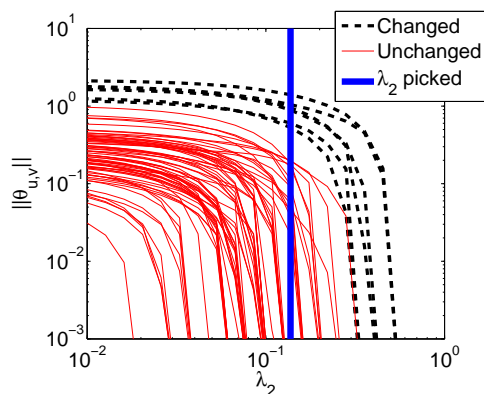
Reflecting a similar pattern, the P-R curves plotted in Figure 7(e) show that the proposed KLIEP method has the best performance among all three methods. We can also see that the IS-Flasso method achieves significant improvement over the plain Flasso method with the Gaussian model. The improvement from Flasso to IS-Flasso shows that the use of the polynomial basis is useful on this dataset, and the improvement from IS-Flasso to KLIEP shows that the direct estimation can further boost the performance.

5.2 Twitter Story Telling

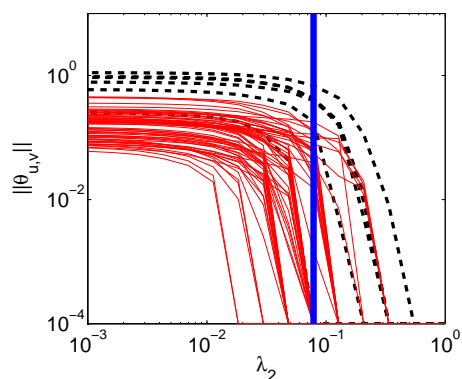
Finally, we use KLIEP with the polynomial transform function for $k \in \{2, 3, 4\}$ and Flasso as event detectors from Twitter. More specifically, we choose the *Deepwater Horizon oil*



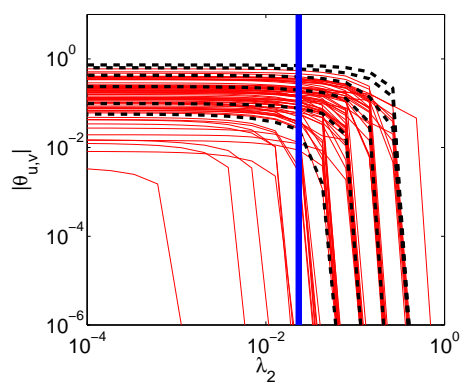
(a) Gene regulatory network



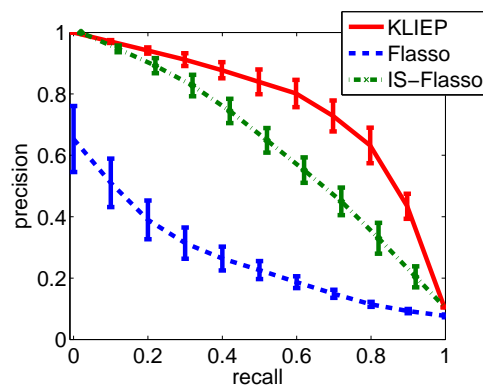
(b) KLIEP



(c) IS-Flasso



(d) Flasso



(e) P-R curve

Figure 7: Experiments on synthetic gene expression datasets.

336 *spill*⁸ as the target event, and we hope that our method can recover some story lines
 337 from Twitter as the news events develop. Counting the frequencies of 10 keywords (BP,
 338 oil, spill, Mexico, gulf, coast, Hayward, Halliburton, Transocean, and Obama), we obtain
 339 a dataset by sampling 4 times per day from February 1st, 2010 to October 15th, 2010,
 340 resulting in 1061 data samples.

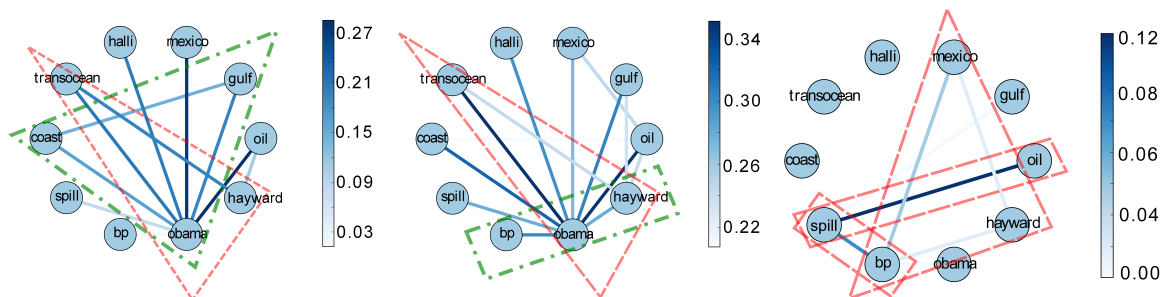
341 We segment the data into two parts: the first 300 samples collected before the day of oil
 342 spill (April 20th, 2010) are regarded as conforming to a 10-dimensional joint distribution
 343 Q , while the second set of samples that are in an arbitrary 50-day window after the
 344 oil spill accident happened is regarded as following distribution P . Thus, the MN of Q
 345 encodes the original conditional independence of frequencies between 10 keywords, while
 346 the underlying MN of P has changed since an event occurred. We expect that unveiling
 347 changes in MNs between P and Q can recover the drift of popular topic trends on Twitter
 348 in terms of the dependency among keywords.

349 The detected change graphs (i.e., the graphs with only detected changing edges) on
 350 10 keywords are illustrated in Figure 8. The edges are selected at a certain value of
 351 λ_2 indicated by the maximal *cross-validated log-likelihood* (CVLL). Since the edge set
 352 that is picked by CVLL may not be sparse in general, we sparsify the graph based on
 353 the permutation test as follows: we randomly shuffle the samples between P and Q and
 354 repeatedly run change detection algorithms for 100 times; then we observe detected edges
 355 by CVLL. Finally, we select the edges that are detected using the original non-shuffled
 356 dataset and remove those that were detected in the shuffled datasets for more than 5
 357 times (i.e., the significance level 5%). For KLIEP, k is also tuned by using CVLL. In
 358 Figure 8, we plot detected change graphs which are generated using samples of P starting
 359 from April 17th, July 6th, and July 26th, respectively.

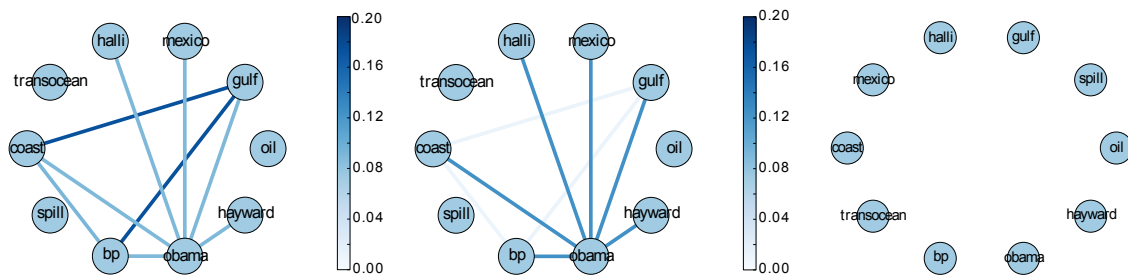
360 The initial explosion happened on April 20th, 2010. Both methods discover depen-
 361 dency changes between keywords. Generally speaking, KLIEP captures more conditional
 362 independence changes between keywords than the Flasso method, especially when com-
 363 paring Figure 8(c) and Figure 8(f). At the first two stages (????????), the keyword
 364 “Obama” is very well connected with other keywords in the results given by both meth-
 365 ods. Indeed, at the early development of this event, he lies in the center of the news stories,
 366 and his media exposure peaks after his visit to the Louisiana coast (May 2nd, May 28nd,
 367 and June 5th) and his meeting with BP CEO Tony Hayward on June 16th. Notably, both
 368 methods highlight the “gulf-obama-coast” triangle in ???? and the “bp-obama-hayward”
 369 chain in ????

370 However, there are some important differences worth mentioning. First, the Flasso
 371 method misses the “transocean-hayward-obama” triangle in ????. Transocean is the con-
 372 tracted operator in the Deepwater Horizon platform, where the initial explosion happened.
 373 On ??, the chain “bp-spill-oil” may indicate that the phrase “bp spill” or “oil spill” has
 374 been publicly recognized by the Twitter community since then, while the “hayward-bp-
 375 mexico” triangle, although relatively weak, may link to the event that Hayward stepped
 376 down from the CEO position on July 27th.

⁸http://en.wikipedia.org/wiki/Deepwater_Horizon_oil_spill



(a) April 17th–June 5th, KLIEP (b) June 6th–July 25th, KLIEP (c) July 26th–Sept. 14th, KLIEP



(d) April 17th–June 5th, Flasso (e) June 6th–July 25th, Flasso (f) July 26th–Sept. 14th, Flasso

Figure 8: Change graphs captured by the proposed KLIEP method (top) and the Flasso method (bottom). The date range beneath each figure indicates when P was sampled, while Q is fixed to dates from February 1st to April 20th. Notable structures shared by the graph of both methods are surrounded by the dash-dotted lines. Unique structures that only appear in the graph of the proposed KLIEP method are surrounded by the dashed lines.

377 It is also noted that Flasso cannot find any changed edges in Figure 8(f), perhaps due
 378 to the Gaussian restriction.

379 6 Discussion, Conclusion, and Future Works

380 In this paper, we proposed a *direct* approach to learning sparse changes in MNs by den-
 381 sity ratio estimation. Rather than fitting two MNs separately to data and comparing
 382 them to detect a change, we estimated the ratio of the probability densities of two MNs
 383 where changes can be naturally encoded as sparsity patterns in estimated parameters.
 384 This direct modeling allows us to halve the number of parameters and approximate the
 385 normalization term in the density ratio model by a sample average without sampling. We
 386 also showed that the number of parameters to be optimized can be further reduced with
 387 the dual formulation, which is highly useful when the dimensionality is high. Through
 388 experiments on artificial and real-world datasets, we demonstrated the usefulness of the
 389 proposed method over state-of-the-art methods including nonparanormal-based methods
 390 and sampling-based methods.

391 Our important future work is to theoretically elucidate the advantage of the proposed
 392 method, beyond the Vapnik’s principle of solving the target problem directly. The relation
 393 to *score matching* (Hyvärinen, 2005), which avoids computing the normalization term in
 394 density estimation, is also an interesting issue to be further investigated. Considering
 395 higher-order MN models such as the *hierarchical log-linear model* (Schmidt and Murphy,
 396 2010) is a promising direction for extension.

397 In the context of change detection, we are mainly interested in the situation where
 398 p and q are close to each other (if p and q are completely different, it is straightforward
 399 to detect changes). When p and q are similar, density ratio estimation for $p(\mathbf{x})/q(\mathbf{x})$
 400 or $q(\mathbf{x})/p(\mathbf{x})$ perform similarly. However, given the asymmetry of density ratios, the
 401 solutions for $p(\mathbf{x})/q(\mathbf{x})$ or $q(\mathbf{x})/p(\mathbf{x})$ are generally different. The choice of the numerator
 402 and denominator in the ratio is left for future investigation.

403 Detecting changes in MNs is the main target of this paper. On the other
 404 hand, estimating the difference/divergence between two probability distributions has
 405 been studied under a more general context in the statistics and machine learning
 406 communities (Amari and Nagaoka, 2000; Eguchi and Copas, 2006; Wang et al., 2009;
 407 Sugiyama et al., 2012b, 2013a). In fact, the estimation of the *Kullback-Leibler diver-*
 408 *gence* (Kullback and Leibler, 1951) is related to the KLIEP-type density ratio estimation
 409 method (Nguyen et al., 2010), and the estimation of the *Pearson divergence* (Pearson,
 410 1900) is related to the squared-loss density ratio estimation method (Kanamori et al.,
 411 2009). However, the density ratio based divergences tend to be sensitive to outliers.
 412 To overcome this problem, a divergence measure based on relative density ratios was
 413 introduced, and its direct estimation method was developed (Yamada et al., 2013). L^2 -
 414 distance is another popular difference measure between probability density functions.
 415 L^2 -distance is symmetric, unlike the Kullback-Leibler divergence and the Pearson diver-
 416 gence, and its direct estimation method has been investigated recently (Sugiyama et al.,
 417 2013b; Kim and Scott, 2010).

418 Change detection in time-series is a related topic. A straightforward approach is
 419 to evaluate the difference (dissimilarity) between two consecutive segments of time-
 420 series signals. Various methods have been developed to identify the difference by fit-
 421 ting two models to two segments of time-series separately, e.g., the singular spectrum
 422 transform (Moskvina and Zhigljavsky, 2003; Ide and Tsuda, 2007), subspace identifi-
 423 cation (Kawahara et al., 2007), and the method based on the one-class support vec-
 424 tor machine (Desobry et al., 2005). In the same way as the current paper, directly
 425 modeling of the change has also been explored for change detection in time-series
 426 (Kawahara and Sugiyama, 2012; Liu et al., 2013; Sugiyama et al., 2013b).

427 Acknowledgements

428 SL is supported by the JST PRESTO program and the JSPS fellowship. JQ is supported
 429 by the JST PRESTO program. MUG is supported by the Finnish Centre-of-Excellence in
 430 Computational Inference Research COIN (251170). TS is partially supported by MEXT

431 Kakenhi 25730013, and the Aihara Project, the FIRST program from JSPS, initiated by
 432 CSTP. MS is supported by the JST CREST program and AOARD.

433 Appendix: Derivation of the Dual Optimization Problem 434 lem

First, we rewrite the optimization problem (??) as

$$\min_{\boldsymbol{\theta}, \mathbf{w}} \left[\log \left(\sum_{i=1}^{n_Q} \exp(w_i) \right) - \boldsymbol{\theta}^\top \mathbf{g} + \frac{\lambda_1}{2} \boldsymbol{\theta}^\top \boldsymbol{\theta} + \lambda_2 \sum_{u \geq v} \|\boldsymbol{\theta}_{u,v}\| - C \right] \quad (10)$$

subject to $\mathbf{w} = \mathbf{H}^\top \boldsymbol{\theta}$,

where

$$\begin{aligned} \mathbf{w} &= (w_1, \dots, w_{n_Q})^\top, \\ \mathbf{H} &= (\mathbf{H}_{1,1}^\top, \dots, \mathbf{H}_{d,1}^\top, \mathbf{H}_{2,2}^\top, \dots, \mathbf{H}_{d,2}^\top, \dots, \mathbf{H}_{d,d}^\top)^\top, \\ \mathbf{H}_{u,v} &= [\mathbf{f}(x_1^{(u)Q}, x_1^{(v)Q}), \dots, \mathbf{f}(x_{n_Q}^{(u)Q}, x_{n_Q}^{(v)Q})], \\ \mathbf{g} &= (\mathbf{g}_{1,1}^\top, \dots, \mathbf{g}_{d,1}^\top, \mathbf{g}_{2,2}^\top, \dots, \mathbf{g}_{d,2}^\top, \dots, \mathbf{g}_{d,d}^\top)^\top, \\ \mathbf{g}_{u,v} &= \frac{1}{n_P} \sum_{i=1}^{n_P} \mathbf{f}(x_i^{(u)P}, x_i^{(v)P}), \\ C &= \log n_Q. \end{aligned}$$

With Lagrange multipliers $\boldsymbol{\alpha} = (\alpha_1, \dots, \alpha_{n_Q})^\top$, the Lagrangian of (??) is given as

$$\begin{aligned} \mathcal{L}(\boldsymbol{\alpha}) &= \min_{\mathbf{w}, \boldsymbol{\theta}} \left[\log \sum_{i=1}^{n_Q} \exp(w_i) - \boldsymbol{\theta}^\top \mathbf{g} + \frac{\lambda_1}{2} \boldsymbol{\theta}^\top \boldsymbol{\theta} + \lambda_2 \sum_{u \geq v} \|\boldsymbol{\theta}_{u,v}\| - (\mathbf{w} - \mathbf{H}^\top \boldsymbol{\theta})^\top \boldsymbol{\alpha} \right] - C \\ &= \min_{\mathbf{w}} \left[\log \sum_{i=1}^{n_Q} \exp(w_i) - \mathbf{w}^\top \boldsymbol{\alpha} \right] \\ &\quad + \min_{\boldsymbol{\theta}} \left[\boldsymbol{\theta}^\top (\mathbf{H} \boldsymbol{\alpha} - \mathbf{g}) + \frac{\lambda_1}{2} \boldsymbol{\theta}^\top \boldsymbol{\theta} + \lambda_2 \sum_{u \geq v} \|\boldsymbol{\theta}_{u,v}\| \right] - C \\ &= \min_{\mathbf{w}} \psi_1(\mathbf{w}) + \min_{\boldsymbol{\theta}} \psi_2(\boldsymbol{\theta}) - C. \end{aligned} \quad (11)$$

A few lines of algebra can show that $\psi_1(\mathbf{w})$ reaches the minimum $-\sum_{i=1}^{n_Q} \alpha_i \log \alpha_i$ at

$$\alpha_i = \frac{\exp(w_i)}{\sum_{i=1}^{n_Q} \exp(w_i)}, \quad i = 1, \dots, n_Q.$$

Note that extra constraints are implied from the above equation:

$$\alpha_1, \dots, \alpha_{n_Q} \geq 0 \text{ and } \sum_{i=1}^{n_Q} \alpha_i = 1.$$

Since $\psi_2(\boldsymbol{\theta})$ is not differentiable at $\boldsymbol{\theta}_{u,v} = \mathbf{0}$, we can only obtain its sub-gradient:

$$\nabla_{\boldsymbol{\theta}_{u,v}} \psi_2(\boldsymbol{\theta}) = -\boldsymbol{\xi}_{u,v} + \lambda_1 \boldsymbol{\theta} + \lambda_2 \nabla_{\boldsymbol{\theta}_{u,v}} \|\boldsymbol{\theta}_{u,v}\|,$$

where

$$\boldsymbol{\xi}_{u,v} = \mathbf{g}_{u,v} - \mathbf{H}_{u,v} \boldsymbol{\alpha},$$

$$\nabla_{\boldsymbol{\theta}_{u,v}} \|\boldsymbol{\theta}_{u,v}\| = \begin{cases} \frac{\boldsymbol{\theta}_{u,v}}{\|\boldsymbol{\theta}_{u,v}\|} & \text{if } \boldsymbol{\theta}_{u,v} \neq \mathbf{0}, \\ \{\mathbf{y} \mid \|\mathbf{y}\| \leq 1\} & \text{if } \boldsymbol{\theta}_{u,v} = \mathbf{0}. \end{cases}$$

435 By setting $\nabla_{\boldsymbol{\theta}_t} \psi_2(\boldsymbol{\theta}) = \mathbf{0}$, we can obtain the solution to this minimization problem by
436 Eq.(??).

437 Substituting the solutions of the above two minimization problems with respect to $\boldsymbol{\theta}$
438 and \mathbf{w} into (??), we obtain the dual optimization problem (??).

439 References

- 440 S. Amari and H. Nagaoka. *Methods of Information Geometry*. Oxford University Press,
441 Providence, RI, USA, 2000.
- 442 O. Banerjee, L. El Ghaoui, and A. d’Aspremont. Model selection through sparse maximum
443 likelihood estimation for multivariate Gaussian or binary data. *Journal of Machine*
444 *Learning Research*, 9:485–516, March 2008.
- 445 C. M. Bishop. *Pattern Recognition and Machine Learning*. Springer, New York, NY,
446 USA, 2006.
- 447 S. Boyd and L. Vandenberghe. *Convex Optimization*. Cambridge University Press, Cam-
448 bridge, UK, 2004.
- 449 P. Danaher, P. Wang, and D. M. Witten. The joint graphical lasso for inverse covariance
450 estimation across multiple classes. *Journal of the Royal Statistical Society: Series B*
451 *(Statistical Methodology)*, 2013.
- 452 F. Desobry, M. Davy, and C. Doncarli. An online kernel change detection algorithm.
453 *IEEE Transactions on Signal Processing*, 53(8):2961–2974, 2005.
- 454 S. Eguchi and J. Copas. Interpreting Kullback-Leibler divergence with the Neyman-
455 Pearson lemma. *Journal of Multivariate Analysis*, 97(9):2034–2040, 2006.

- 456 J. Friedman, T. Hastie, and R. Tibshirani. Sparse inverse covariance estimation with the
457 graphical lasso. *Biostatistics*, 9(3):432–441, 2008.
- 458 A. Gelman. Method of moments using Monte Carlo simulation. *Journal of Computational
459 and Graphical Statistics*, 4(1):36–54, 1995.
- 460 M. U. Gutmann and A. Hyvärinen. Noise-contrastive estimation of unnormalized statisti-
461 cal models, with applications to natural image statistics. *Journal of Machine Learning
462 Research*, 13:307–361, 2012.
- 463 T. Hastie, R. Tibshirani, and J. Friedman. *The Elements of Statistical Learning: Data
464 Mining, Inference, and Prediction*. Springer, New York, NY, USA, 2001.
- 465 G. E. Hinton. Training products of experts by minimizing contrastive divergence. *Neural
466 computation*, 14(8):1771–1800, 2002.
- 467 A. Hyvärinen. Estimation of non-normalized statistical models by score matching. *Journal
468 of Machine Learning Research*, 6:695–709, 2005.
- 469 T. Ide and K. Tsuda. Change-point detection using Krylov subspace learning. In *Pro-
470 ceedings of the SIAM International Conference on Data Mining*, pages 515–520, 2007.
- 471 T. Kanamori, S. Hido, and M. Sugiyama. A least-squares approach to direct importance
472 estimation. *Journal of Machine Learning Research*, 10:1391–1445, 2009.
- 473 T. Kanamori, T. Suzuki, and M. Sugiyama. Theoretical analysis of density ratio esti-
474 mation. *IEICE Transactions on Fundamentals of Electronics, Communications and
475 Computer Sciences*, E93-A(4):787–798, 2010.
- 476 Y. Kawahara and M. Sugiyama. Sequential change-point detection based on direct density-
477 ratio estimation. *Statistical Analysis and Data Mining*, 5(2):114–127, 2012.
- 478 Y. Kawahara, T. Yairi, and K. Machida. Change-point detection in time-series data based
479 on subspace identification. In *Proceedings of the 7th IEEE International Conference on
480 Data Mining*, pages 559–564, 2007.
- 481 J. Kim and C. Scott. L_2 kernel classification. *IEEE Transactions on Pattern Analysis
482 and Machine Intelligence*, 32(10):1822–1831, 2010.
- 483 D. Koller and N. Friedman. *Probabilistic Graphical Models: Principles and Techniques*.
484 MIT Press, 2009.
- 485 S. Kullback and R. A. Leibler. On information and sufficiency. *The Annals of Mathemat-
486 ical Statistics*, 22:79–86, 1951.
- 487 S.-I. Lee, V. Ganapathi, and D. Koller. Efficient structure learning of Markov networks
488 using l_1 -regularization. In B. Schölkopf, J. Platt, and T. Hoffman, editors, *Advances
489 in Neural Information Processing Systems 19*, pages 817–824, Cambridge, MA, 2007.
490 MIT Press.

- 491 H. Liu, J. Lafferty, and L. Wasserman. The nonparanormal: Semiparametric estimation
492 of high dimensional undirected graphs. *Journal of Machine Learning Research*, 10:
493 2295–2328, 2009.
- 494 H. Liu, F. Han, M. Yuan, J. Lafferty, and L. Wasserman. The nonparanormal skeptic. In
495 *Proceedings of the 29th International Conference on Machine Learning (ICML2012)*,
496 2012.
- 497 S. Liu, M. Yamada, N. Collier, and M. Sugiyama. Change-point detection in time-series
498 data by relative density-ratio estimation. *Neural Networks*, 43:72–83, 2013.
- 499 N. Meinshausen and P. Bühlmann. High-dimensional graphs and variable selection with
500 the lasso. *The Annals of Statistics*, 34(3):1436–1462, 2006.
- 501 V. Moskvina and A. Zhigljavsky. Change-point detection algorithm based on the singular-
502 spectrum analysis. *Communications in Statistics: Simulation and Computation*, 32:
503 319–352, 2003.
- 504 R. M Neal. Slice sampling. *The Annals of Statistics*, 31(3):705–741, 2003.
- 505 X. Nguyen, M. J. Wainwright, and M. I. Jordan. Estimating divergence functionals and
506 the likelihood ratio by convex risk minimization. *IEEE Transactions on Information
507 Theory*, 56(11):5847–5861, 2010.
- 508 K. Pearson. On the criterion that a given system of deviations from the probable in the
509 case of a correlated system of variables is such that it can be reasonably supposed to
510 have arisen from random sampling. *Philosophical Magazine*, 50:157–175, 1900.
- 511 P. Ravikumar, M. J. Wainwright, and J. D. Lafferty. High-dimensional Ising model selec-
512 tion using ℓ_1 -regularized logistic regression. *The Annals of Statistics*, 38(3):1287–1319,
513 2010.
- 514 C. P. Robert and G. Casella. *Monte Carlo Statistical Methods*. Springer-Verlag, Secaucus,
515 NJ, USA, 2005.
- 516 M. W. Schmidt and K. P. Murphy. Convex structure learning in log-linear models: Beyond
517 pairwise potentials. *Journal of Machine Learning Research - Proceedings Track*, 9:709–
518 716, 2010.
- 519 M. Sugiyama, T. Suzuki, S. Nakajima, H. Kashima, P. von Bünau, and M. Kawanabe.
520 Direct importance estimation for covariate shift adaptation. *Annals of the Institute of
521 Statistical Mathematics*, 60(4):699–746, 2008.
- 522 M. Sugiyama, T. Suzuki, and T. Kanamori. *Density Ratio Estimation in Machine Learn-
523 ing*. Cambridge University Press, Cambridge, UK, 2012a.

- 524 M. Sugiyama, T. Suzuki, and T. Kanamori. Density-ratio matching under the Bregman
525 divergence: a unified framework of density-ratio estimation. *Annals of the Institute of*
526 *Statistical Mathematics*, 64(5):1009–1044, 2012b.
- 527 M. Sugiyama, S. Liu, M. C. du Plessis, M. Yamanaka, M. Yamada, T. Suzuki, and
528 T. Kanamori. Direct divergence approximation between probability distributions and
529 its applications in machine learning. *Journal of Computing Science and Engineering*, 7
530 (2):99–111, 2013a.
- 531 M. Sugiyama, T. Suzuki, T. Kanamori, M. C. du Plessis, S. Liu, and I. Takeuchi. Density-
532 difference estimation. *Neural Computation*, 25(10):2734–2775, 2013b.
- 533 R. Tibshirani, M. Saunders, S. Rosset, J. Zhu, and K. Knight. Sparsity and smooth-
534 ness via the fused lasso. *Journal of the Royal Statistical Society: Series B (Statistical*
535 *Methodology)*, 67(1):91–108, 2005.
- 536 Y. Tsuboi, H. Kashima, S. Hido, S. Bickel, and M. Sugiyama. Direct density ratio es-
537 timation for large-scale covariate shift adaptation. *Journal of Information Processing*,
538 17:138–155, 2009.
- 539 T. Van den Bulcke, K. Van Leemput, B. Naudts, P. van Remortel, H. Ma, A. Verschoren,
540 B. De Moor, and K. Marchal. SynTReN: A generator of synthetic gene expression data
541 for design and analysis of structure learning algorithms. *BMC Bioinformatics*, 7(1):43,
542 2006.
- 543 V. N. Vapnik. *Statistical Learning Theory*. Wiley, New York, NY, USA, 1998.
- 544 M. J. Wainwright and M. I. Jordan. Graphical models, exponential families, and varia-
545 tional inference. *Foundations and Trends® in Machine Learning*, 1(1-2):1–305, 2008.
- 546 Q. Wang, S. R. Kulkarni, and S. Verdú. Divergence estimation for multidimensional
547 densities via k-nearest-neighbor distances. *IEEE Transactions on Information Theory*,
548 55(5):2392–2405, 2009.
- 549 L. Wasserman. *All of Statistics: A Concise Course in Statistical Inference*. Springer
550 Publishing Company, Incorporated, 2010.
- 551 M. Yamada, T. Suzuki, T. Kanamori, H. Hachiya, and M. Sugiyama. Relative density-
552 ratio estimation for robust distribution comparison. *Neural Computation*, 25(5):1324–
553 1370, 2013.
- 554 B. Zhang and Y.J. Wang. Learning structural changes of Gaussian graphical models in
555 controlled experiments. In *Proceedings of the Twenty-Sixth Conference on Uncertainty*
556 *in Artificial Intelligence (UAI2010)*, pages 701–708, 2010.
- 557 H. Zou and T. Hastie. Regularization and variable selection via the elastic net. *Journal*
558 *of the Royal Statistical Society, Series B*, 67(2):301–320, 2005.